INTEGRATING DENSITY-BASED UNCERTAINTY PROPAGATION WITH OBJECT-ORIENTED RE-ENTRY MODELS

Mirko Trisolini[(1)] **and Camilla Colombo**[(2)]

[(1)]*Politecnico di Milano, via La Masa 34, 20156, Milano, Italy, Email: mirko.trisolini@polimi.it*
[(2)]*Politecnico di Milano, via La Masa 34, 20156 Milano, Italy, Email: camilla.colombo@polimi.it*

ABSTRACT

In this work, the effect of uncertainties in the re-entry and break-up of satellites is combined with a destructive re-entry analysis of object-oriented codes. The approach used to model the re-entry and propagate the relevant uncertainties is based on the continuity equation, where the uncertainty probability density is propagated alongside the trajectory to predict its evolution in time. The propagation can only be done for discrete points in the state space so that density reconstruction must be performed. This is achieved using the Starling suite developed at the Politecnico di Milano. The developed framework is integrated with an object-oriented approach so that the uncertainties related to the parent spacecraft re-entry, the break-up, and the child components re-entry are considered in a comprehensive fashion. The framework is applied to relevant test cases of uncontrolled re-entries and the results.

Keywords: re-entry, demise, object-oriented, gaussian mixture models, casualty risk.

1. INTRODUCTION

The analysis fo the re-entry of space objects and of the possible effects they may have on people and properties on the ground is an important task. In fact, when a spacecraft re-enter the Earth's atmosphere, operators must ensure that the casualty risk on ground derived by possible surviving fragments is lower than the well-known limit of 10^{-4} for uncontrolled re-entries. The compliance with this regulation has also to be verified during the design and development phases of a space missions. This ultimately means that a spacecraft can be disposed via uncontrolled re-entry only if its design guarantees a casualty risk below the aforementioned threshold. In case this is not possible, more expensive controlled re-entry strategies must be employed. To verify the compliance of a spacecraft design, operators and manufacturers perform analyses using destructive re-entry codes, which analyse the demise of the spacecraft and predicts the landing of the surviving fragments, together with their casualty risk. Among these software suite, the most commonly used are the so-called *object-oriented* models [2, 4, 19, 21, 20, 22]. With these kinds of codes, the spacecraft is schematised in a hierarchical fashion subdividing the main spacecraft structure (the *parent*) from the internal components (the *children*). All the components are modelled using basic geometrical shapes and the aero-thermodynamics loads are assessed via engineering correlations and averaging factors. These types of codes are in general deterministic and rely on Monte Carlo techniques to perform uncertainty analyses, running a large number of simulations changing initial conditions and relevant parameters.

In this work, we explore the possibility of interfacing the deterministic nature of object-oriented codes with the statistically-based continuum propagations. In a continuum propagation, the uncertainty probability density associated to the uncertainties is propagated alongside the equations of motion, using the continuity equation, so that the actual evolution of the probability density is available as a function of space and time. Such a methodology has been already applied to the propagation of interplanetary dust, swarms of satellites, Earth orbiting fragments derived from collisions, and in re-entry applications [6, 12, 17, 18, 3]. In this work, this methodology is subsequently applied to the different phases that characterise object-oriented simulations. First, to the propagation of the parent spacecraft until break-up. Then, to model the break-up event describing a random impulse given to the internal components by the erratic behaviour and the explosion occurring at break-up. Finally, to the analysis of the internal components until they reach the ground or demise. When using the continuum propagation, the value of the density is only known at discrete points in the state space. Therefore, a reconstruction methodology must be used to obtain the uncertainty distribution in the entire domain. In this work, a fitting is performed using the Starling suite developed at the Politecnico di Milano, which is currently based on Gaussian Mixture Models (GMM) [3]. The current work si based on previous works [17, 18] and expands on them by introducing the mass loss dynamics into the equations of motion and the density conservation equation. The challenges and limitations of introducing such equation for the propagation and the continuity hypothesis are discussed. The continuum propagation and the reconstruc-

tion methodology using Starling is applied to a relevant example, highlighting the capabilities of the methodology and its integration with object-oriented codes. The difference between the implementations with and without including the mass loss to the dynamics is also discussed.

2. METHODOLOGY

This section outlines the methodology used in this work, which is based on a continuum approach to uncertainty propagation and its interface with object-oriented destructive re-entry codes. First, a brief overview of object-oriented re-entry codes is given and the possibility of interfacing the continuum propagation its discussed. Subsequently, the continuum-based methodology is described, together with the dynamical model used in the present work.

2.1. Object-oriented destructive re-entry codes

Object-oriented destructive re-entry codes are used in the field of re-entry to predict the level of demise of a re-entering object and assess its possibility to be a threat for people and properties on the ground [13, 14, 10, 19, 20, 21, 23, 22]. They are routinely used by national and international space agencies to perform risk assessment of re-entry campaign and check the compliance of spacecraft with the casualty risk regulations. In general, the main features of these types of codes are:

- Hierarchical spacecraft definition;
- Schematisation of components and structures with primitive shapes (cube, cylinder, sphere, and flat plate);
- Use of engineering correlations for aerodynamics and aerothermodynamics interactions.

The first hierarchical level is the main spacecraft structure (the *parent object*). Here the overall spacecraft mass and dimensions are specified. In addition, the solar panels can be defined and schematised as flat plates. The re-entry simulation of the solar panels is not performed and they are assumed to demise; however, their area is taken into account in the computation of the aerodynamic cross-section of the satellite until they detached at a user specified altitude [5, 4, 11]. The second level defines the main internal components and subsystems such as tanks and reaction wheels assemblies. Additional levels can be used for the definition of sub-components such as battery cells.

The simulation of an object-oriented code can be broadly divided into three parts. A first part that only takes into account the parent spacecraft, until the main break-up altitude is reached. In this phase, only the parent structure can interact with the external heat flux. It is assumed that the internal components do not experience any heat load during this phase. A second part that simulates the main break-up of the spacecraft. In this case, the user usually sets a threshold that triggers the break-up such as the altitude or the heat load for example. Usually, the internal components are then released with the same state as the parent at the break-up instant. However, additional break-up conditions, such as small impulses that can further scatter the internal components can be modelled [18, 9]. After the break-up, the internal components are released and their trajectory and demise analysed.

In the present work, these three phases that characterise object-oriented codes, are tackled from a continuum point of view. With this respect, uncertainties are included in each one of these phases. First, the uncertainties related to the parent spacecraft are taken into account until break-up. Subsequently, the break-up is modelled via break-up model, which describes the impulse given at the break-up via a distribution function, which is combined with the uncertainties of the parent spacecraft. This combination results in the initial conditions for the propagation of the internal components. The internal components are then propagated taking into account their uncertainties.

2.2. Continuum-based propagation

As previously mentioned, the proposed methodology is based on the continuum approach for the propagation of the probability density of re-entry uncertainties. This can be obtained applying the continuity equation to the specific dynamical problem in exam.

$$\frac{\partial n(\mathbf{x},t)}{\partial t} + \nabla \cdot \mathbf{f}(\mathbf{x}) = \dot{n}^{+} - \dot{n}^{-}, \tag{1}$$

where $n(\mathbf{x},t)$ is the density at time t and state $\mathbf{x}$, $\nabla \cdot \mathbf{f}(\mathbf{x})$ represents the forces acting on the system from slow, continuous phenomena such as gravity and atmospheric drag, and $\dot{n}^{+} - \dot{n}^{-}$ represents the fast and discontinuous events (sources and sinks). For the case in exam, the source and sink terms are neglected. Knowing the probability density distribution at the initial time, $n(\mathbf{x},0)$, Eq. (1) allows the propagation of the density evolution in time. This is a Partial Differential Equation (PDE) with the joint Probability Distribution Function (PDF) $n(\mathbf{x},t)$ being the dependent variable. Such an equation regulates the conservation of the total probability mass of the joint PDF through its spatial-temporal evolution due to the forces acting on the system.

Eq. (1) can be solved using the Method of Characteristics (MOC), where the partial differential equation is transformed into a set of Ordinary Differential Equations (ODE) as follows [6]:

$$\begin{cases} \frac{\mathrm{d}\alpha_1}{\mathrm{d}s} = v_{\alpha_1}(\alpha_1, \ldots, \alpha_m) \\ \ldots \\ \frac{\mathrm{d}\alpha_m}{\mathrm{d}s} = v_{\alpha_m}(\alpha_1, \ldots, \alpha_m) \\ \frac{\mathrm{d}n}{\mathrm{d}s} = -\left[\frac{\partial v_{\alpha_1}}{\partial \alpha_1} + \cdots + \frac{\partial v_{\alpha_m}}{\partial \alpha_m}\right] n(\alpha_1, \ldots, \alpha_m) \end{cases} \tag{2}$$

where s is the independent variable, $(\alpha_1, \ldots, \alpha_m)$ are the state variables of the system. It is possible to observe how the evolution of the density is regulated by the trace of the Jacobian of the dynamics describing the system.

As it is convenient to express the evolution of the re-entry trajectory using re-entry parameters, we specialize Eq. (2) to the re-entry problem, where we have used the radius as the independent variable.

where λ is the longitude, φ the latitude, v the velocity, γ the flight-path angle, $\beta = \frac{m}{C_D S}$ the ballistic coefficient, $\alpha = \frac{C_L S}{m}$ a modified lift coefficient of the re-entering object, and g_r and g_φ are the radial and transversal components of the gravitational acceleration, respectively. The expression for the derivative of the density as a function of r has not been expanded for a better readability.

In this expression, the primes refers to partial derivatives with respect to the radius. Any gravitational and atmospheric model can be used, as long as they can be modeled with a continuous and differentiable function. For the case in exam, the 1976 US Standard Atmosphere [15] was considered for the atmosphere and a model including the effects of the Earth oblateness for the gravitational acceleration [16].

The system of Eq. (3) has to be numerically integrated. The integration can be performed using a standard ODE solver such as the Runge-Kutta method. In such fashion, the time evolution of the density in the considered state space can be obtained for a specified set of time instants. As the solution for the re-entry problem is not analytical, it is necessary to sample the initial density distribution and to integrate the system of Eq. (3) for each one of the sampled points. Subsequently, the distribution can be reconstructed at each time step by fitting the scattered data over the state space domain.

The dynamics of Eq. (3) can be used to describe the motion of a component under uncertainties when its mass is not changing. This type of dynamics can be used to analyse the motion of the parent spacecraft and of those internal components that tend not to demise, such as the ones made of high melting point materials (e.g. titanium alloys, ceramics).

2.2.1. Components demise

For components made with materials with lower heat resistance, it is necessary to include the mass variation inside the equations of motion. In the current work the mass variation is considered by using a lumped mass model [17, 22]. Eq. (4) describes the variation of mass with the radius as this is the independent variable chosen for this work.

$$m' = \begin{cases} -\frac{A_w}{h_f v \sin\gamma}(F_q \dot{q} - \epsilon\sigma T^4) & \text{if } Q \geq Q_m \\ 0 & \text{elsewhere} \end{cases} \tag{4}$$

where A_w is the component wet area, h_f is the material heat of fusion, ϵ is the material emissivity, σ is the Stefan-Boltzman constant, T is the temperature in Kelvin, $\dot{q}$ is the conductive heat rate acting on the component, and F_q is a shape factor that takes into account the shape and motion of the components. Shape factors are commonly used in combination of engineering correlations to estimate the average heat rate on a component of a given shape and motion. The contribution of $v \sin\gamma$ is included to convert the independent variable from time to radius. Q and Q_m are the integral heat load on the component and the integral heat load required to reach the melting temperature respectively. If we consider temperature independent material properties, Q_m can be expressed as follows:

$$Q_m = m c_p (T_m - T_0), \tag{5}$$

where m is the mass of the object, c_p the heat capacity at constant pressure of the material of the object, and T_m and T_0 are the melting temperature and initial temperature, respectively. The initial temperature is commonly set to 300 K. The condition in Eq. (4) expresses the common fact that, in a lumped mass model, the object starts to lose mass only after the melting temperature is reached.

The expression of the heat rate, $\dot{q}$, is based on the Detra-Kemp-Riddel correlation as follows [22]:

$$\dot{q} = 1.99876 \times 10^8 \sqrt{\frac{0.3048}{r_n}} \sqrt{\frac{\rho}{\rho_{SL}}} \left(\frac{v}{7924.8}\right)^{3.15} \tag{6}$$

where r_n is the nose radius of the component, ρ is the free-stream density, ρ_{SL} is the sea-level atmospheric density and v is the free-stream velocity. The temperature dependence in Eq. (4) is considered in a simplified fashion. The temperature can be expressed as $T = \min\left(T_0 + Q/(mc_p),\ T_m\right)$, where the integral heat load Q can be integrated together with the set of equations of motion.

Including Eq. (4) into the continuum approach presents also the added difficulty that such expression is not continuous. In fact, a discontinuity is presented by the fact the the mass loss is null before the component reaches the melting temperature, and abruptly switch to a finite value once the melting temperature is reached. To tackle

$$
\begin{cases}
\frac{\mathrm{d}\lambda}{\mathrm{d}r} = \frac{\sin(\chi)}{r\cos(\varphi)\tan(\gamma)} \\
\frac{\mathrm{d}\varphi}{\mathrm{d}r} = \frac{\cos(\chi)}{r\tan(\gamma)} \\
\frac{\mathrm{d}v}{\mathrm{d}r} = -\frac{v\rho(r)}{2\beta\sin(\gamma)} - \frac{1}{v}\left(g_r(r,\varphi) + \frac{\cos(\chi)g_\varphi(r,\varphi)}{\tan(\gamma)}\right) + \frac{r\omega_p^2\cos(\varphi)}{v}\left(\cos(\varphi) - \frac{\cos(\chi)\sin(\varphi)}{\tan(\gamma)}\right) \\
\frac{\mathrm{d}\gamma}{\mathrm{d}r} = \frac{\alpha\rho(r)}{2\sin(\gamma)} - \frac{1}{v^2\tan(\gamma)}\left(g_r(r,\varphi) + \cos(\chi)\tan(\gamma)g_\varphi(r,\varphi) - \frac{v^2}{r}\right) + \frac{2\omega\sin(\chi)\cos(\varphi)}{v\sin(\gamma)} + \\
\qquad + \frac{r\omega_p^2\cos(\varphi)}{v}\left(\frac{\cos(\varphi)}{\tan(\gamma)} + \cos(\chi)\sin(\varphi)\right) \\
\frac{\mathrm{d}\chi}{\mathrm{d}r} = \frac{\sin(\chi)\tan(\varphi)}{r\tan(\gamma)} + \frac{2\omega_p}{v}\left(\frac{\sin(\varphi)}{\sin(\gamma)} - \frac{\cos(\chi)\cos(\varphi)}{\cos(\gamma)}\right) + \\
\qquad + \frac{\sin(\chi)}{v^2\sin(\gamma)\cos(\gamma)}\left(r\omega_p^2\sin(\varphi)\cos(\varphi) - g_\varphi(r,\varphi)\right) \\
\frac{\mathrm{d}\beta}{\mathrm{d}r} = 0 \\
\frac{\mathrm{d}n}{\mathrm{d}r} = -\left[\frac{\partial\lambda'}{\partial\lambda} + \frac{\partial\varphi'}{\partial\varphi} + \frac{\partial v'}{\partial v} + \frac{\partial\gamma'}{\partial\gamma} + \frac{\partial\chi'}{\partial\chi} + \frac{\partial\beta'}{\partial\beta}\right]n
\end{cases}
\tag{3}
$$

this issue, a simple yet effective method, is to halt the propagation once the threshold is met and restart it. This procedure allows for the conservation of the probability density throughout the motion, including the demise dynamics into the set of equations of motion.

Of course, the inclusion of Eq. (4) into the equations of motions, also requires to take care of the evolution of the probability density, which in turns consists into adding a component to the trace of the Jacobian. However, in this case, Eq. (4) does not directly depend on the mass, so that we have

$$
\frac{\partial m'}{\partial m} = 0. \tag{7}
$$

Therefore, adding the lumped mass model to the dynamics does not directly change the equation governing the evolution of the density.

2.3. Break-up uncertainties

As introduced in Section 2.1, in object oriented code the modelling phases also include the break-up of the parent spacecraft and the subsequent dispersion of the internal components. In this work, we take into account the break-up of the parent spacecraft using a probability distribution to generate a delta-V impulse that is given to the internal components at the break-up instant. We use a probability function to describe such a behaviour as it can take into account the uncertainties in the process and is also perfectly integrate with the philosophy of the continuum approach. For this work, the break-up induced impulse is modelled via the NASA Standard Break-up Model (SBM) [8]. This model has been originally developed for in-orbit breakups and its use in re-entry simulation is a preliminary extrapolation. Nonetheless, the NASA SBM has already been adopted in ESA DRAMA to describe the possible explosions and consequent fragmentation of components during re-entry [5]. In that context it was used by directly sampling the distribution to generate the fragments in a Monte Carlo fashion. In this case, it is used to model the ejection velocity and direction that can be imparted to a component during the break-up event.

The NASA SBM models the ejection velocity of a component at break-up through a log-normal distribution as follows:

$$
p_{\Delta v}(\chi,\nu) = \mathcal{N}(\mu(\chi),\sigma(\chi),\nu), \tag{8}
$$

where $\mathcal{N}$ is a Normal distribution, $\chi = \log_{10}(A/M)$ is the logarithm in base ten of the area-to-mass ratio, $\nu = \log_{10}(\Delta v)$, and $\mu(\chi) = 1.85 + 0.2\cdot\chi$ and $\sigma(\chi) = 0.4$ are the mean and standard deviation of the Normal distribution. Here, the coefficients for explosions of the NASA SBM have been used.

Eq. (8) provides the expression for probability distribution of Δv as a function of ν. The first step is thus to transform it into an expression as a function of Δv as follows:

$$
p_{A/M,\Delta v}(A/M,\Delta v) = \frac{p_{\Delta v}(\chi,\nu)}{\log(10)^2\cdot\Delta v\cdot A/M}. \tag{9}
$$

where $p_{\Delta v}(\chi,\nu)$ is the distribution obtained from the NASA SBM in the variables χ and ν, $Deltav$ is the impulse imparted to the object, and A/M is the area-to-mass ratio of the object. The probability value $p_{\Delta v}(\Delta v)$ can be then obtained by marginalization of Eq. (9). The Δv provided by the NASA SBM only gives the absolute value of the impulse; however, to properly model the break-up we consider that the ejection can happen randomly in any direction relative to the S/C re-entry velocity. Therefore, the provided impulse is transformed into

a vector quantity $\Delta\mathbf{v} = (\Delta v_x, \Delta v_y, \Delta v_z)$, where the x axis is oriented along the North direction, the z axis is oriented along the radial direction, ant the y axis comes from applying the right-hand rule (Fig. 1).

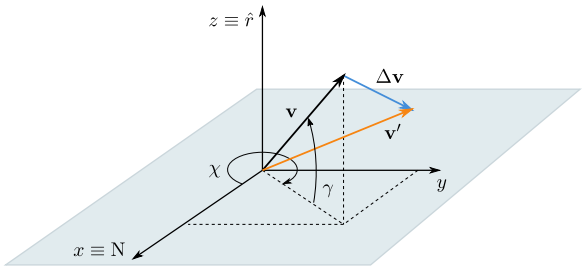

Figure 1: Reference frame for the velocity decomposition to compute the velocity after the break-up impulse.

The decomposition of the absolute velocity into its components, requires a transformation of the probability density of Eq. (8) as follows:

$$p_{\Delta\mathbf{v}}(\Delta\mathbf{v}) = \frac{p_{\Delta v}(\Delta v)}{4\pi\Delta v^2}, \tag{10}$$

The contribution of the $\Delta\mathbf{v}$ impulse is then combined to the velocity of the object before the break-up event. In this way, we obtain a fully statistical description of the event. The velocity of the internal component after the break-up will thus be a combination of the parent velocity and the break-up impulse given by the NASA SBM.

$$\begin{cases} \hat{v} = \sqrt{(v_x + \Delta v_x)^2 + (v_y + \Delta v_y)^2 + (v_z + \Delta v_z)^2} \\ \hat{\gamma} = \tan\left(\frac{v_z + \Delta v_z}{\sqrt{(v_x+\Delta v_x)^2 + (v_y+\Delta v_y)^2}}\right)^{-1} \\ \hat{\chi} = \tan\left(\frac{v_y + \Delta v_y}{v_x + \Delta v_x}\right)^{-1} \end{cases} \tag{11}$$

where $\hat{v}$, $\hat{\gamma}$, and $\hat{\chi}$ are the velocity magnitude, flight-path angle, and heading angle after the break-up, and v_x, v_y, and v_z are the same components before the break-up, expressed in the same reference frame as the Δv components, which can be expressed as follows:

$$\begin{cases} v_x = v\cos\gamma\cos(2\pi - \chi) \\ v_y = v\cos\gamma\sin(2\pi - \chi) \\ v_z = v\sin\gamma \end{cases} \tag{12}$$

To overlap the break-up distribution with the parent distribution, consider the parent spacecraft at break-up point has an uncertainty distribution $p(v, \gamma, \chi)$, and that the impulse uncertainty $p_{\Delta\mathbf{v}}(\Delta\mathbf{v})$ is independent from this state. We can then create an extended probability distribution as follows:

$$p(v, \gamma, \chi, \Delta v_x, \Delta v_y, \Delta v_z) = p(v, \gamma, \chi) \cdot p(\Delta\mathbf{v}). \tag{13}$$

Applying Eq. (11) and using the Dirac generalized transformation we can obtain the distribution in the new variables after the break-up ($\hat{v}$, $\hat{\gamma}$, $\hat{\chi}$) in Eq. (14), where $\det J(\varphi)$ is the determinant of the Jacobian of the transformation of Eq. (11).

The values of v_x, v_y, and v_z are then obtained inverting the transformation of Eq. (11).

3. APPLICATION TO THE OBJECT-ORIENTED PARADIGM

In this section, the methodology described in Section 2 is applied to a test case with a typical object-oriented simulation pipeline. Recalling Section 2.1, the pipeline is essentially constituted by three phases: the parent spacecraft simulation, the break-up event, and the internal component analysis. In the following section, we will show the application of the continuum approach to each of these sections.

3.1. Parent spacecraft simulation

As previously mentioned, we first simulate the trajectory of the parent spacecraft. The trajectory starts from an altitude of 120 km and is propagated up to a standard break-up altitude of 78 km. The initial conditions and relevant simulation parameters are summarised in Table 1.

Table 1: Mean and standard deviation for the initial conditions of the parent spacecraft and values of the relevant parameters.

Initial state	Symbol	Unit	μ	σ
Longitude	λ_0	°	10.0	0.2
Latitude	φ_0	°	0.0	0.2
Velocity	v_0	km/s	7.6	0.012
Flight-path angle	γ_0	°	-1.5	0.05
Heading angle	χ_0	°	90	0.2
Parameter	**Symbol**	**Unit**	**Value**	
Initial altitude	h_0	km	120	
Ballistic coeff.	β	kg/m^2	500.0	
Lift coefficient	α	m^2/kg	0.0	

The trajectory of the parent spacecraft is then simulated using Eq. (3) up to the break-up altitude. After the simulation, at each time step, we have the evolution of the parent trajectory and its associated uncertainty density. As the probability is only known at discrete point, a fitting is required, which is performed using the Starling suite [3] developed at the Politecnico di Milano, which is based on Gaussian Mixture Models. Fig. 2 shows an example of the distribution reconstructed with Starling at the predefined break-up altitude of 78 km.

$$p(\hat{v},\hat{\gamma},\hat{\chi}) = \int p(v_x,v_y,v_z,\Delta\mathbf{v})\ \delta(\hat{v}-\varphi_1)\ \delta(\hat{\gamma}-\varphi_2)\delta(\hat{\chi}-\varphi_3)\ dv_x\, dv_y dv_z\, d\Delta\mathbf{v}$$
$$= \iiint \frac{p(\hat{v},\hat{\gamma},\hat{\chi},\Delta\mathbf{v})}{|\det J(\varphi)|}\, d\Delta v_x\, d\Delta v_y\, d\Delta v_z, \tag{14}$$

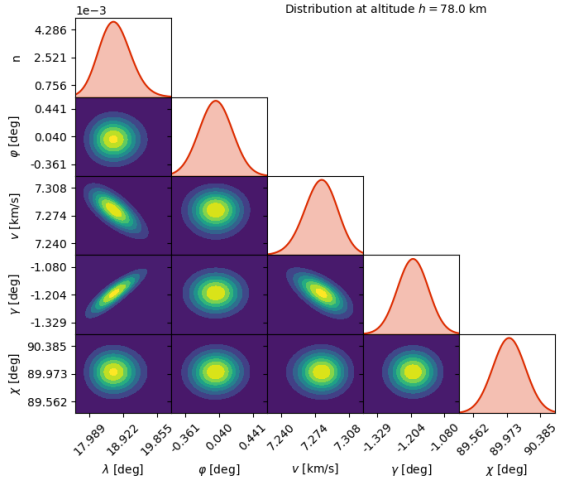

Figure 2: Snapshot fit using Starling at the break-up altitude of 78 km.

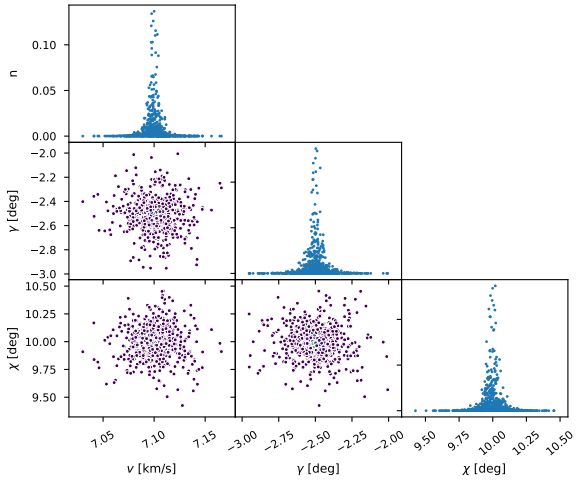

Figure 3: Break-up distribution in v, γ, χ obtained with the procedure of Section 2.3.

3.2. Break-up event

To model the break-up event, we combine the snapshot of Fig. 2 with a the delta-V impulse distribution obtained from the NASA SBM as described in Section 2.3. To obtain the distribution it is also necessary to provide the area-to-mass ratio of the considered component. The component selected for this test case is a reaction wheel, which is a component that usually survives re-entry. The characteristics of the considered reaction wheel are summarised in Table 2.

Table 2: Characteristics of the reaction wheel used in the test case.

State	Symbol	Unit	Value
Diameter	D	cm	15.66
Height	H	cm	6.26
Mass	m	kg	9.5
Drag coefficient	C_D		1.535
Cross-section (average)	S	m^2	0.0161

Fig. 3 shows an example of the initial conditions obtained sampling the break-up distribution obtained from Eq. (14). This is only a subset of the state space, limited to the (v, γ, χ) variables, as they are the only ones affected by the break-up. Latitude and longitude are left unchanged as the break-up event is assumed instantaneous.

From the figure we can observe a distribution with a fairly localised peak around the average values of velocity, flight-path angle and heading angle. This is a result of the sampling from a log-normal distribution. It is also a reasonable distribution as we can expect the impulse given by the break-up event to be smaller than the velocity of the spacecraft, which is in the order of kilometres per second.

3.3. Internal components analysis

Once the initial conditions for the internal components after break-up have been obtained following the procedure of Section 3.2, we can analyse their re-entry trajectory. The procedure is analogous to the one of the parent spacecraft: the trajectory is propagate using Eq. (3) for 500 sampled points and then reconstructed at each snapshot using the Starling suite. Fig. 4 shows an example of the fitting results obtained using Starling, for the landing snapshot. In the figure, the off diagonal plots represent the scatter data points used in the fitting, while the orange crosses represent the position of the kernels of the GMM surrogate model. The diagonal plots instead show the marginals obtained using Starling in orange, and the corresponding histogram approximated using Monte Carlo. The results of the fitting are comparable to the Monte Carlo simulation.

The advantage of the Starling approach is the possibility to retrieve the uncertainty distribution and its marginals as a continuum function that is a sum of Gaussian kernels. This is a considerable advantage for the post-processing of the results. We present here an application in which

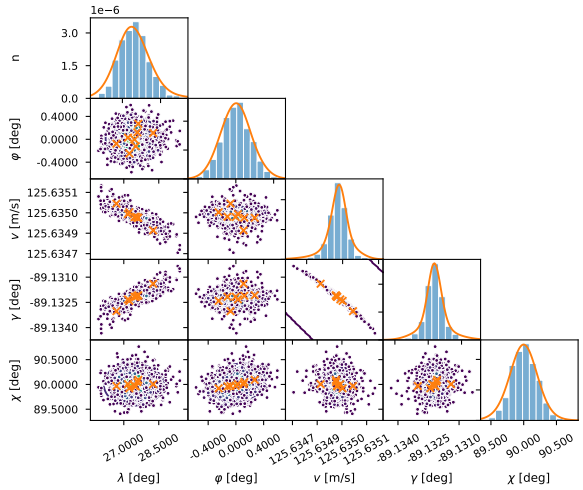

Figure 4: Landing snapshot fit using Starling. The orange crosses are the kernel locations of the Gaussian distributions. On the main diagonal plots a comparison between the marginal obtained with the fitting (in orange) and the histogram obtained with Monte Carlo.

the marginal in longitude and latitude hs been extracted from the landing snapshot and combined with the Gridded World population [1] to compute the casualty risk. In fact, by multiplying the landing probability at a location with the population density and the cross-section of the component we can obtain a risk map, an example of which is shown in Fig. 5.

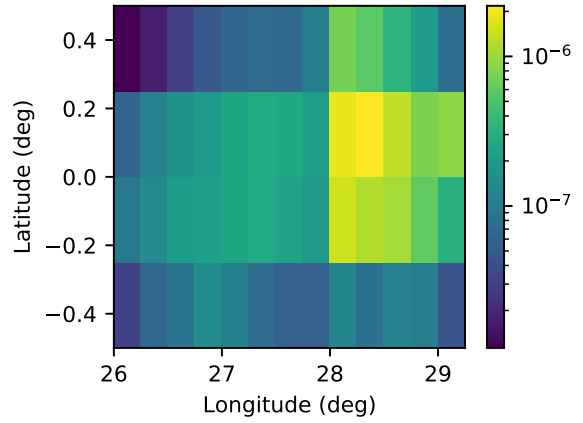

Figure 5: Casualty risk distribution for the reaction wheel test case.

3.4. Demisability analysis

The previous example has been obtained considering that the object is not subject to mass loss. As this is not necessarily the case for several internal components, it is necessary to include the the mass variation into the equations of motion Eq. (4). Given the nature of the continuum approach, in order to add the mass to the propagation, it is necessary to add to the initial distribution an uncertainty in the mass parameter, which is then propagated together with the probability density. For the case in exam, the standard deviation associated to the mass is $\sigma_m = 0.1\ kg$, for an average mass equal to the one of the previous case and reported in Table 2. The considered material is the stainless steel AISI304 with the following properties:

Table 3: AISI304 material properties.

Variable	Symbol	Unit	Value
Density	ρ_m	$\mathrm{kg/m^3}$	7900
Melting temp.	T_m	K	1650
Heat of fusion	h_f	J/kg	286098
Heat capacity	C_p	J/kg/K	545
Emissivity	ϵ		0.35

Such a component and material combination has been selected as it allows to have a simulation in which the mass starts to decrease at a certain point during the re-entry, but the component does not completely demise. Instead, when the heat load is not sufficient any more, the demise stops and the mass does not vary any more. An example of this behaviour is presented in Fig. 6, where we can observe the stable evolution of the probability density until an altitude of about 55 km, with the mass stable around the mean value of 9.5 kg. Once a certain altitude is reached, the component starts to lose mass. As expected, the mass loss is concentrated in a relatively small altitude interval. In fact, the mass loss stops at an altitude of about 45 km, and remains stable until the end of the propagations.

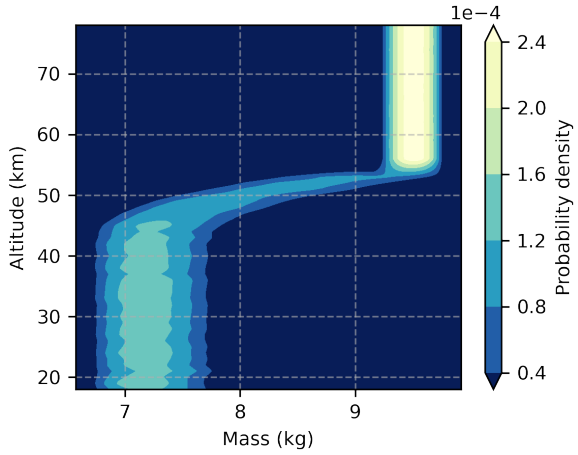

Figure 6: Mass distribution variation as a function of the altitude.

It is possible to observe in Fig. 6 that the simulations stops just below an altitude of 20 km. Differently to the previous test case (Section 3.3), where the full trajectory had been solved and fitted with Starling, in this case, the fitting was achieved until an altitude of 18 km. Below this altitude, the GMM surrogate model of Starling could not converge. Fig. 7 shows the evolution of the probability integral obtained from the fitting with Starling.

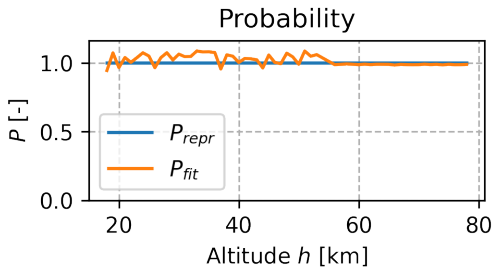

Figure 7: Evolution of the total probability as a function of the altitude.

It is evident from the figure that the stability of the fitting is high in the initial part of the trajectory, right up until the mass loss starts. When this happens, the fitting is still stable but the value of the total integral has higher oscillations. This behaviour indicates that including the mass loss equation into the continuum dynamics reduces the stability of the fitting. This is possibly due to the non-continuous nature of Eq. (4), to the extension of the state space, which is now six-dimensional instead of five-dimensional, and to the added non-linearities introduced by the change of mass during the propagation.

Fig. 8 shows an example of a snapshot that the GMM surrogate model of starling was not able to fit. It is interesting to discriminate between the physical state space of the propagation and the space in which Starling performs the fitting. The lower-triangular part of the plot represents the actual physical space. It is possible to observe how some of the variables, velocity, flight-path angle and mass, show a strong correlation. This correlation becomes stronger as the propagation progresses and can be among the reasons for a reduced fitting stability. In fact, in general, it is difficult for fitting and interpolation routines to deal with these types of domains. The upper-triangular part of the plot is, instead, the space in which Starling performs the fitting to the GMM. This space is obtained via a standardisation and principal component decomposition of the state space. This is a standard pre-processing procedure to improve the stability of fitting routines. In this case, however, the non-linearities introduced by the re-entry dynamics generate a domain that is difficult to fit for GMM surrogate models. In fact, the highly distorted, non-Gaussian behaviour, together with bounded set of points make this type of domain challenging to fit for Starling. Possible mitigation measures may be taken to improve the quality and stability of the fitting. Examples are a variable transformation or the dimensionality reduction, exploiting the correlations that forms during the propagation between some of the variables in play.

4. CONCLUSIONS

The presented work has outlined a methodology to propagate and reconstruct re-entry uncertainties using the continuity equation and Gaussian Mixture Models and its integration with object-oriented codes: from the parent simulation, to the internal components analysis, passing through the modelling of the break-up event. In addition, the mass loss dynamics has been included into the equations of motion. The models were applied to a representative test case in which a spacecraft trajectory is propagated until break-up and its uncertainties are then used in combination with a break-up model to obtain the initial conditions for the release of an internal component. In this particular case, the re-entry of a reaction wheel has been considered. The results show that the continuum propagation combined with the Starling suite is able to capture the evolution of the trajectory and its uncertainties with a limited number of samples. In addition, the marginal distribution in longitude and latitude can be readily obtained and used for the prediction of the on-ground casualty risk. This is achieved by combining the resulting landing probability with the population density in the same area and the casualty area of the surviving fragment, giving a more realistic and statistically sound prediction. The same test case has then been applied including the contribution of the mass loss. The propagation and reconstruction has been achieved until an altitude of about 20 km, with a good fitting stability. It has been observed how the mass loss introduces some difficulties in the propagation and fitting of the probability density. First, the mass loss equation has a discontinuity, which must be properly included into the continuum propagation, for example, by stopping and re-starting the integration. Secondly, including the mass both extend the dimension of the state space to be fitted and introduces further non-linearities that make the fitting more challenging. Nonetheless, the methodology has been integrated with the object-oriented paradigm. Its application can be still explored, possibly considering alternatives to the fitting via GMM surrogate models [7].

ACKNOWLEDGMENTS

This project has received funding from the European Research Council (ERC) under the European Union's Horizon 2020 research and innovation programme (grant agreement No 679086 - COMPASS).

REFERENCES

1. Center for International Earth Science Information Network (CIESIN). Gridded Population of the World, Version 4 (GPWv4), 2018. URL `https://doi.org/10.7927/H4PN93PB`. Accessed: 2020-06-20.

2. J. Dobarco-Otero, R. Smith, K. Bledsoe, R. Delaune, W. Rochelle, and N. Johnson. The object reentry survival analysis tool (orsat)-version 6.0 and its application to spacecraft entry. In *Proceedings of the 56th Congress of the International Astronautical Federation, the International Academy of Astronautics, and*

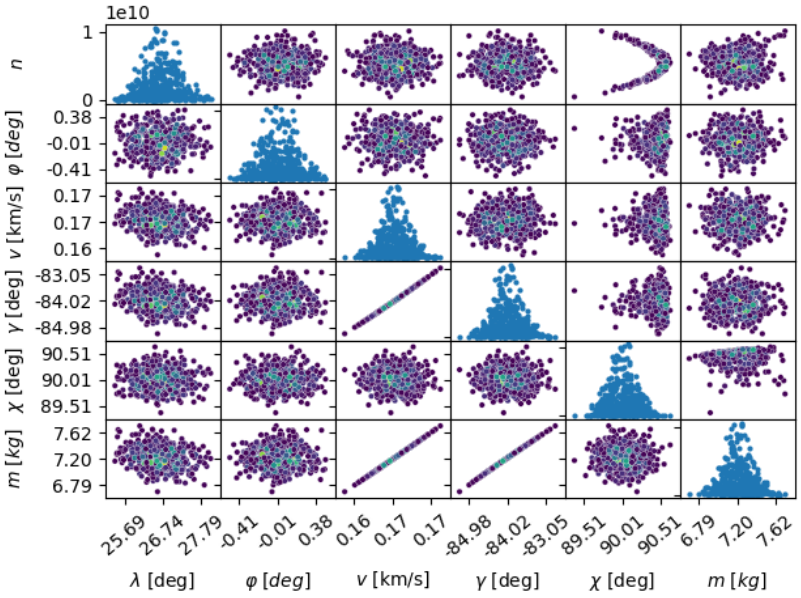

Figure 8: Example of snapshot with unsuccessful fitting. Physical state space in the lower-triangular part. Fitting space in the upper-triangular part.

International Institute of Space Law, IAC-05-B6, volume 3, pages 17–21, 2005.

3. S. Frey, C. Colombo, S. Lemmens, et al. Application of density-based propagation to fragment clouds using the starling suite. In *1st International Orbital Debris Conference (IOC)*, pages 1–10, 2019.
4. J. Gelhaus, N. Sanchez-Ortiz, V. Braun, C. Kebschull, J. C. de Oliveira, R. Dominguez-Gonzalez, C. Wiedemann, H. Krag, and P. Vorsmann. Upgrade of DRAMA-ESA's Space Debris Mitigation Analysis Tool Suite. In *ESA Special Publication*, volume 723, page 62, 2013. ISBN 1609-042X.
5. J. Gelhaus, C. Kebschull, V. Braun, N. Sanchez-Ortiz, E. Parilla Endrino, J. C. de Oliveira, and R. Dominguez-Gonzalez. Upgrade of ESA's Space Debris Mitigation Analysis Tool Suite. Technical Report ESA contract 4000104977/11/D/SR, European Space Agency, 2014.
6. N. N. Gor'kavyi, L. M. Ozernoy, and J. C. Mather. A New Approach to Dynamical Evolution of Interplanetary Dust. *The Astrophysical Journal*, 474 (1):496–502, jan 1997. ISSN 0004-637X. doi: 10.1086/303440.
7. A. Halder and R. Bhattacharya. Dispersion Analysis in Hypersonic Flight During Planetary Entry Using Stochastic Liouville Equation. *Journal of Guidance, Control, and Dynamics*, 34(2):459–474, 2011. doi: 10.2514/1.51196.
8. N. L. Johnson, P. Krisko, J.-C. Liou, and P. Anz-Meador. Nasa's new breakup model of evolve 4.0. *Advances in Space Research*, 28(9):1377–1384, 2001.
9. S. Limonta, M. Trisolini, S. Frey, and C. Colombo. Modelling the break-up and re-entry propagation of meteorites through a continuum approach. Number IAC-20-C1.2.10, oct 2020.
10. T. Lips and B. Fritsche. A comparison of commonly used re-entry analysis tools. *Acta Astronautica*, 57:312–323, 2005. doi: 10.1016/j.actaastro.2005.03.010. URL `http://search.ebscohost.com/login.aspx?direct=true{&}db=edselp{&}AN=S0094576505000767{&}site=eds-live`.
11. C. E. Martin, J. E. Cheeses, N. Sanchez-Ortiz, H. Klinkrad, K. Bunte, S. Hauptmann, B. Fritsche, and T. Lips. Introducing the ESA DRAMA tool. *Science and Technology Series*, 110:219–233, 2005.
12. C. R. McInnes. Autonomous ring formation for a planar constellation of satellites. *Journal of Guidance, Control, and Dynamics*, 18(5):1215–1217, 1995. ISSN 07315090. doi: 10.2514/3.21531.
13. National Astronautics and Space Administration. ORSAT, 2009. URL `http://orbitaldebris.jsc.nasa.gov/reentry/orsat.html`.
14. National Astronautics and Space Administration. Debris Assessment Software, 2015. URL `http://orbitaldebris.jsc.nasa.gov/mitigate/das.html`.
15. National Oceanic and Atmospheric Administration. U.S. Standard Atmosphere 1976, 1976.
16. A. Tewari. *Atmospheric and Space Flight Dynamics: Modeling and Simulation with MATLAB® and Simulink®*. Birkhäuser, 2007. ISBN 9780817644383.
17. M. Trisolini and C. Colombo. A density-based approach to the propagation of re-entry uncertainties. In *29th AAS/AIAA Space Flight Mechanics Meeting*, pages 1–13, Ka'anapali, Hawaii, USA, 2019.

18. M. Trisolini and C. Colombo. Modeling re-entry break-up uncertainties with continuity equation and Gaussian mixture models interpolation. In *Proceedings of the 2020 AAS/AIAA Astrodynamics Specialist Conference*, pages AAS 20–636, 2020.

19. M. Trisolini, H. G. Lewis, and C. Colombo. Survivability and Demise Criteria for Sustainable Spacecraft Design. In *66th International Astronautical Conference*, Jerusalem, 2015.

20. M. Trisolini, H. G. Lewis, and C. Colombo. Demise and Survivability Criteria for Spacecraft Design Optimization. *Journal of Space Safety Engineering*, 3 (2):83–93, 2016. ISSN 24688967. doi: 10.1016/S2468-8967(16)30023-4.

21. M. Trisolini, H. G. Lewis, and C. Colombo. Demisability and survivability multi-objective optimisation for preliminary spacecraft design. In *68th International Astronautical Congress*, Adelaide, Australia, 2017.

22. M. Trisolini, H. G. Lewis, and C. Colombo. Spacecraft design optimisation for demise and survivability. *Aerospace Science and Technology*, 77:638–657, jun 2018. ISSN 12709638. doi: 10.1016/j.ast.2018.04.006.

23. M. Trisolini, H. G. Lewis, and C. Colombo. Demisability and survivability sensitivity to design-for-demise techniques. *Acta Astronautica*, 145:357–384, 2018. doi: 10.1016/j.actaastro.2018.01.050.